HOKKAIDO UNIVERSITY

Title	Revisiting Activity Tuning Using Lattice Strain : CO Decomposition in Terrace Ru(0001) and Stepped Ru(1015) Surfaces
Author(s)	De Chavez, Danjo; Hasegawa, Jun-ya
Citation	Journal of physical chemistry c, 126(22), 9324-9333 https://doi.org/10.1021/acs.jpcc.2c00902
Issue Date	2022-06-09
Doc URL	https://hdl.handle.net/2115/89683
Rights	This document is the Accepted Manuscript version of a Published Work that appeared in final form in The Journal of Physical Chemistry C, copyright © American Chemical Society after peer review and technical editing by the publisher. To access the final edited and published work see http://pubs.acs.org/articlesonrequest/AOR-9SBEKXWPZKQCWK2XX4TP
Type	journal article
File Information	Manuscript.pdf

Hokkaido University Collection of Scholarly and Academic Papers : HUSCAP

Revisiting Activity Tuning using Lattice Strain: CO Decomposition in Terrace Ru(0001) and Stepped Ru(1015) Surfaces

Danjo De Chavez[*,†,‡] and Jun-ya Hasegawa[*,‡]

†*Graduate School of Chemical Sciences and Engineering, Hokkaido University, N13W8, Kita-Ku, Sapporo 060-0810, Japan*

‡*Institute for Catalysis, Hokkaido University, N21W10, Kita-Ku, Sapporo 001-0021, Japan*

E-mail: dechavezdanjo@cat.hokudai.ac.jp; hasegawa@cat.hokudai.ac.jp

Abstract

To understand the influence of incongruent strain on heterogeneous catalysis, the effect of isotropic and anisotropic strains in the catalytic activity of terrace Ru(0001) and stepped Ru(1015) surfaces have been studied for the initial step of Fischer-Tropsch (FT) reaction. Adsorption-strain relations have been investigated using the d-band model and the novel eigenstress model. The adsorption relation in the reactant state follows both models. The eigenstress model can predict similar qualitative changes in the adsorption energies without the need to calculate the d-band center of the slab. Activation energies also scale according to Brønsted-Evans-Polyani (BEP) relation. Some exemptions included new minimum energy pathways which do not break the scaling relations but reinforces the mechanochemical effect of producing new chemical pathways with the strain. In addition, in the case of a compressed Ru(1015) surface, reactant adsorption energy does not scale with dissociation activation energy. This is explained by the heightened difference in the reactant interaction energy. These results offer a potential novel route to break the BEP relation in catalysis.

Introduction

Fischer-Tropsch (FT) reaction is an industrially relevant reaction route used to produce long chain saturated and unsaturated hydrocarbons which utilizes carbon monoxide as the primary carbon source.[1,2] Two mechanisms have been proposed and can be seen in the literature: (1) Direct CO dissociation and (2) Hydrogen-assisted CO activation. In the direct dissociation pathway, CO decomposition preferentially occurs on the step-edge sites of the metal surface. While in the hydrogen-assisted pathway occurs preferentially on the terrace sites. It should be noted that at high coverage, it was shown both in experiments and in simulations, that CO activation proceeds via a hydrogen-assisted pathway.[3–5] FT reaction starts with the adsorption of carbon monoxide (CO) to a metal surface. The general FT reaction scheme for ethylene and ethane is given as Figure 1. Conventional catalysts used

in such applications are ruthenium (Ru),[3,5–10] iron (Fe),[11–14] nickel (Ni),[15,16] and cobalt (Co).[17–20]

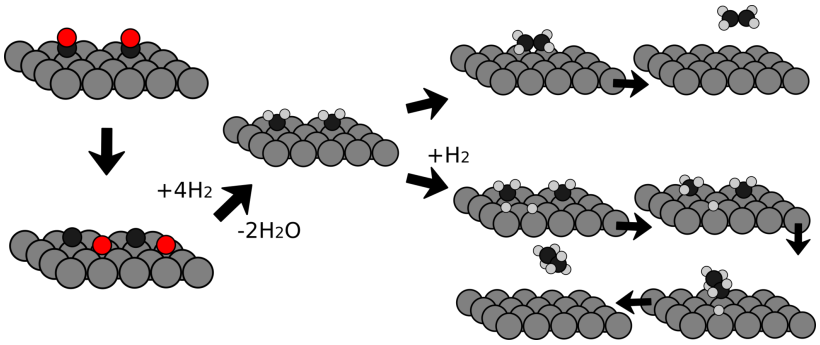


Figure 1: Reaction scheme of Fischer-Tropsch process for ethane and ethylene formation.

Strain engineering has been utilized to control the activity of several catalytic and functional materials.[21] It has been predicted based on the d-band model that compression leads to lesser binding energy to adsorbate, while expansion contributes to greater binding energy. Because of the adsorption scaling relations, activation and reaction energies are also affected accordingly. Brønsted-Evans-Polyani (BEP) relation describes the linear relation which exists between activation energy (E_a) and reaction energy (ΔH_R).[22] While the analogue for transition state energy (E_TS) and reactant/product energy (ΔE) scaling is referred as Transition State Scaling (TSS) relation.[23] BEP and TSS relations are given in their equation forms as Eqs. 1 and 2, respectively, where α_BEP, β_BEP, α_TSS, and β_TSS are constants.

$$E_\mathrm{a} = \alpha_\mathrm{BEP}\Delta H_\mathrm{R} + \beta_\mathrm{BEP} \tag{1}$$

$$E_\mathrm{TS} = \alpha_\mathrm{TSS}\Delta E + \beta_\mathrm{TSS} \tag{2}$$

Catalytic activity tuning via lattice strain is not a very novel concept and has been used in CO oxidation, oxygen reduction reaction, to give a few examples.[24–26] Recently, it was shown that the paradigm offered by the conventional BEP relation can also be circumvented by strain.[27,28] The potential of strain to break the scaling relation stems from the difference in adsorbate-surface interaction during the reaction progression. During the relaxation to

the optimum adsorption conformation, the adsorbate exerts either an attractive or repulsive force to the surface. The force exerted by the adsorbate to the surface results in a lattice strain on the adsorption site. Consequently, the surface exerts force to adsorbate inducing molecular geometry changes. These adsorbate-surface interactions can be amplified or reduced by an externally induced lattice strain. The interplay of the adsorption-attributed strain as well as the external material scale strain can result in the tuning of reaction energetics. As the reaction progresses, the geometric transition from the reactant to the product is accompanied by a change in surface interaction. A schematic of the concept is given as Fig. 2. An incongruent change in the interaction from reactant to product via the corresponding transition state can lead to the non-linear relations in reaction energetics. However, computational catalysts screening normally assumes scaling relationship with respect to strain effects.

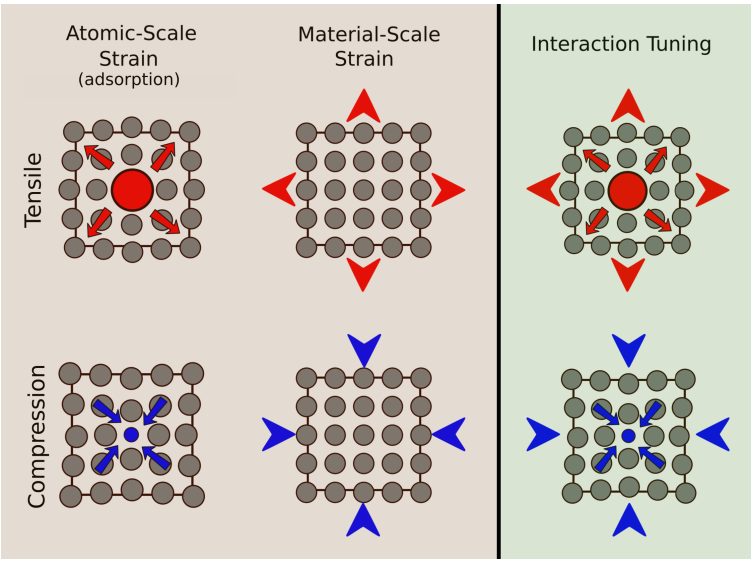


Figure 2: Potential of strain to tune reactivity and break scaling relations. Adapted by permission from Springer Nature: Nature Catalysis (Mechanochemistry breaks with expectations, J. Weissmüller), 2018.

The surface adsorption energy is conventionally discussed by the d-band model which requires the calculation of d-band center of the metal surface.[29] An alternative model to assess the effect of compressive and tensile strain have recently been formulated by Khorshidi

and colleagues which was coined as eigenstress model.[27] Eigenstress model requires only the nuclear forces on the optimized adsorption complex in relaxed surfaces. Details of which will be further discussed later on this paper.

The objective of this work is to explore the effect of isotropic and anisotropic strain in the catalytic activity for direct CO dissociation of Ru by sampling the relevant minimum energy pathways in Ru(0001) and Ru(1015) surfaces and its implications to the BEP relationship. Furthermore, adsorption energies are analyzed using both the conventional d-band model and the novel eigenstress model. It should be noted that Ru-based catalysts are not commercially used in FT reactors due to its high price. Affordable alternatives such Fe and Co based materials are used instead. However, the conceptual understanding and results from this study can be easily be extended to the related Fe and Co systems.

Methods

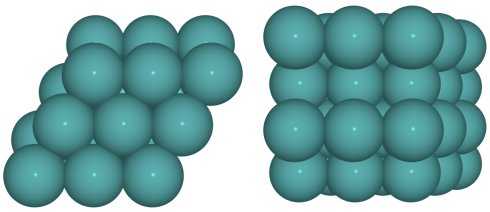
In this work, density functional theory (DFT) calculations are carried out using the GPAW package[30–32] accompanied by the Atomic Simulation Environment (ASE).[33] Using the available generalized gradient approximation (GGA) DFT functionals, it was determined that the revised Perdew–Burke–Ernzerhof (RPBE) functional, coupled with converged calculation parameters, afforded the closest crystal lattice parameters in comparison to the experimental values, and hence RPBE was chosen to account for the exchange-correlation.[34,35] The RPBE performance is expected as previous studies have also determined experimentally comparable lattice constants and energetics using this functional.[3,5,7,36,37]

GPAW calculations were done in the plane-wave mode with an energy cutoff of 700 eV and real space grid spacing parameter h of 0.2, corresponding to 5 grid points per 1 Å. Self-consistent energies and its derivatives were achieved with Pulay density mixing using beta constant of 0.2 and 10 percent weight from 10 previous SCF iterations.[38,39] Brillouin zone sampling for ruthenium unit cells converged with a Monkhorst-Pack 12x12x12 k-point

grid.[40] These parameters are determined from bench-marking calculations.

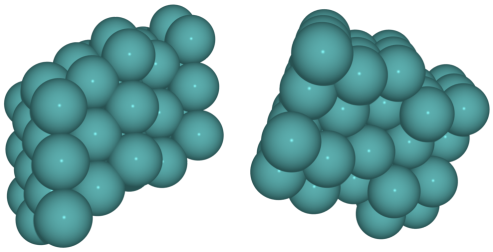
To model ruthenium terrace sites, a 3x3 slab Ru(0001) surface was used. The Monkhorst-Pack k-point grid for the unit cell was scaled according to the surface model size, and hence we employed a 4x4x1 k-point grid.[40] Other calculation parameters are retained. Change in surface energy converged to < 0.01 meV/A using 4 layers and hence, was used throughout the study.[22,41] Optimized Ru(0001) surface structure is illustrated in Figures 3(a) and 3(b) at normal and lateral perspectives, respectively.

I. Terrace Ru(0001)

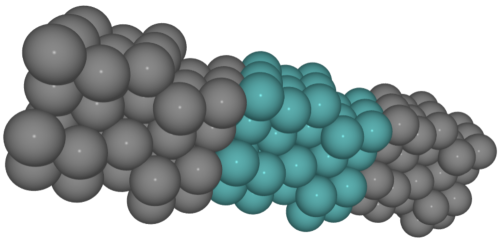


(a) normal view (b) lateral view

II. Stepped Ru(1015)



(c) normal view (d) lateral view



(e) repeated along the lattice vector $\boldsymbol{a}$

Figure 3: Optimized structures of terrace Ru(0001) in the (a) normal and (b) lateral views, and stepped Ru(1015) in the (c) normal, (d) lateral views, and (e) repeated along lattice vector $\boldsymbol{a}$.

It is well known that the step sites of Ru surfaces is important for its catalytic activity.[42,43] The step sites were modeled using the Ru(1015) surface as illustrated in Figures 3(c) and 3(d). This model can be physically described as a Ru(0001) surface having step sites without kink sites. Similar to the terrace model, converged k-point sampling was scaled; hence, 2x4x1 k-point grid was used for all calculations for this surface. Number of layers was chosen to be similar to the terrace model along the Ru(0001) area of stepped Ru(1015) surface model. To demonstrate the stepped structure of the Ru(1015) surface, the unit cell is repeated along the lattice vector $\boldsymbol{a}$ and illustrated in Figure 3(e).

In this study, both isotropic and anisotropic strains were considered. Prior to the introduction of strain, Poisson ratio was determined. Poisson ratio is the quotient of the relative contraction strain to the relative extension strain which can be calculated as

$$\mu = -\frac{\epsilon_{\text{transverse}}}{\epsilon_{\text{lateral}}} \tag{3}$$

where $\epsilon_{\text{transverse}}$ is the strain along the direction of the applied force or constraint while the $\epsilon_{\text{lateral}}$ is that of along the perpendicular direction. Strain ϵ is defined as the ratio of the change in length (ΔL) and original length (L_{o}), that is

$$\epsilon = \frac{\Delta L}{L_{\text{o}}} \tag{4}$$

At 3% expansion or compression, the calculated Poisson ratio is 0.31, which is comparable to the experimental value of 0.30.[44] This can be interpreted that the physical changes due to the isotropic and anisotropic strain can be modeled using the calculation parameters described above. Details of Poisson ratio calculation is given in the Supporting Information (SI). Additionally, the compressibility of the model material was also calculated using the Murnaghan equation of state (EOS),[45,46] and is determined to be 292 GPa. Murnagahan EOS plot is appended as Figure S1 in the SI. This value is closer to the experimental value of 220 GPa than the reported value of 330 GPa in the Materials Project.[47] Materials Project

is a consolidation of different theoretical calculations. This shows that the energetics of the strained cells are better described using our current calculation methods compared to the method described in the Materials Project.

To achieve strained surface models, ±3% strain was applied. The previously optimized lattice constants were adjusted according to the ideal μ and geometry optimizations were done. Isotropic mode employed lattice constraints in both $\boldsymbol{a}$ and $\boldsymbol{b}$ cell parameters. Anisotropic mode employed lattice constraints only in a single lattice constant. For the terrace Ru(0001) slab model which has the same $\boldsymbol{a}$ and $\boldsymbol{b}$ constant, constraints were imposed along the $\boldsymbol{a}$ direction only, producing 5 unique slabs. On the other hand, the stepped Ru(1015) slab does not share the same symmetry and hence constraints were done along $\boldsymbol{a}$ and $\boldsymbol{b}$ separately, resulting in 7 unique slabs. This computational method can also applicable in studying geometric effects in core-shell nanoparticles. In such systems, lattice mismatch of the core or support material induces lattice strain in the shell region. Explicit addition of the core material would include the combined geometric and electronic effects of the core to the thermodynamics of the catalyst model. To study geometric effects separately, a strained lattice model described above can be utilized.

To calculate for the minimum energy pathways, climbing image nudged elastic band (CI-NEB) calculations were done by interfacing to Atomic Simulation Environment (ASE) with GPAW as the quantum chemical calculator while using the converged parameters described above.[33] Dynamic optimization and force scaling were used to hasten convergence of CI-NEB calculations.[48–50] CI-NEB path optimization was considered converged when the maximum atomic force is less than 0.05 eV/bohr.

Results & Discussion

Adsorption energy under applied strain

To initiate this study, we investigated the carbon monoxide adsorption energetics in the terrace Ru(0001) slab model. In this slab, there are four unique adsorption sites: (a) on-top, (b) bridge, (c) hexagonal-close pack (hcp), and (d) face-centered cubic (fcc) sites. These sites are illustrated in a diagram in Figure 4. The adsorption energy calculations were done using a single CO molecule for both Ru(0001) and Ru(1015) models.

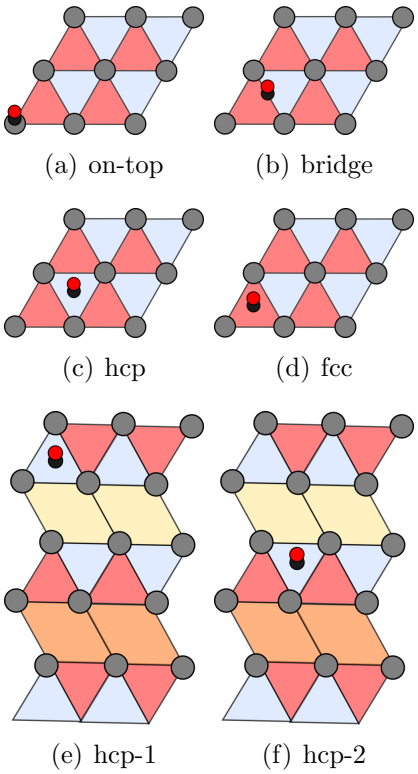


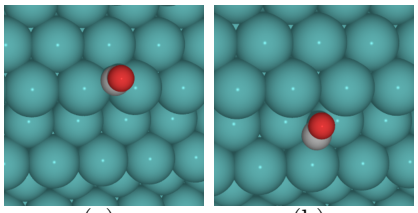
Figure 4: Adsorption sites in (a-d) terrace Ru(0001) and (e-f) stepped Ru(1015). On-top (gray), hcp (blue), fcc (red), step (yellow/orange) sites are shown with different colors. Red and black circles represent O and C atoms, respectively.

Adsorption energy was calculated as

$$E_{\text{ads}} = E_{\text{complex}} - E_{\text{CO}} - E_{\text{slab}} \tag{5}$$

where E_{complex}, E_{CO} and E_{slab} are the energy of the optimized CO-slab complex, CO and Ru slab, respectively.

Our calculation results showed a preferential adsorption on the on-top site with -37.9 kcal mol^{-1} which corresponds to the experiment at low coverage. This is followed by hcp with -32.9 kcal mol^{-1}, bridge with -31.3 kcal mol^{-1} and fcc with -31.0 kcal mol^{-1}. As these values are similar with each other, it can be considered that the CO molecule is mobile along the terrace sites. Similar discussion was done by other computational studies.[37,51]



(a) (b)

Figure 5: CO adsorption geometries at (a) hcp-1 (b) hcp-2 sites in relaxed Ru(0015) surface. Red, gray, and green atoms are O, C, and Ru atoms, respectively.

Adsorption energies were also calculated for the stepped Ru(1015) surface. As seen in Figure 4, there are many unique adsorption sites in the model. Adsorption sites were limited to 2 unique hcp sites as illustrated in Figures 4(e) and 4(f). The difference in these sites is their chemical environments. Figure 4(e) corresponds to a step-edge site, while Figure 4(f) directly interacts with the stepped surface.

From the calculated adsorption energies, the uniqueness of these sites is demonstrated. It shows that the step-edge site has higher binding energies in comparison to the other. Corresponding adsorption geometries are given in Figure 5. Note that the CO at the hcp-2 site is oriented laterally to the step site. This induces a decrease in the effective overlap of CO molecular orbital to the metal d-orbitals during adsorption. The calculated adsorption energies in the hcp-1 and hcp-2 sites are -35.3 kcal mol^{-1} and -30.6 kcal mol^{-1}, respectively. Adsorption energies are summarized in Tables 1 and 2 for Ru(0001) and Ru(1015), respectively with entry label Relaxed.

Prior to studying the CO dissociation reaction on both models, the effect of strain to

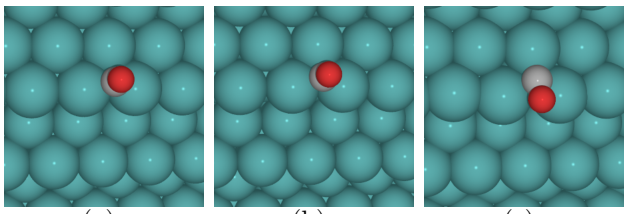
Table 1: CO adsorption energies (kcal·mol^{-1}) at different adsorption sites in relaxed and strained Ru(0001).

Slab	on-top	bridge	hcp	fcc
Relaxed	-38.0	-31.3	-32.9	-31.0
Isotropic Expansion	-40.3	-39.0	-35.8	-33.3
Isotropic Compression	-36.6	-29.1	-30.1	-28.5
Anisotropic Expansion	-38.8	-31.8	-33.8	-33.8
Anisotropic Compression	-37.1	-29.9	-32.0	-30.1

Table 2: CO adsorption energies (kcal·mol^{-1}) at different adsorption sites in relaxed and strained Ru(1015).

Slab	hcp-1	hcp-2
Relaxed	-35.3	-30.6
Isotropic Expansion	-36.5	-33.3
Isotropic Compression	-33.9	-25.7
Anisotropic Expansion in a	-35.7	-31.9
Anisotropic Compression in a	-35.0	-29.1
Anisotropic Expansion in b	-35.7	-31.0
Anisotropic Compression in b	-35.2	-30.0

adsorption energies was investigated. It is notable that adsorption geometries are generally maintained with the exemption of step-edge sites where relaxed and expanded cells have an upright CO orientation with respect to the normal vector of the step site, while the compressed cells have CO tilted towards the edge of the step. This can be seen in Figure 6 where the CO orientation in Figure 6(c) differs with Figures 6(a) and 6(b). This trend is also seen in anisotropically compressed lattices.

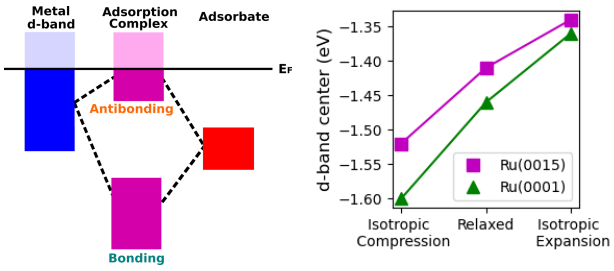


(a) (b) (c)

Figure 6: CO adsorption geometries at step-edge site of (a) relaxed, (b) isotropically expanded, and (c) isotropically compressed Ru(0015) surface. Red, gray, and green atoms are O, C, and Ru atoms, respectively.

d-band model and eigenstress analysis

It is generally accepted that the adsorption energy of a molecule to a metal surface scales with the d-band center of the associated metal.[29] This is known as the d-band model given as Figure 7(a). The said model summarizes the contribution of metal orbitals to the adsorption in a single parameter, the d-band center. According to the d-band model, the d-band center of the metal surface should lie at higher energies to achieve a stronger adsorption. In contrast, adsorbents with a low-lying d-band center would have weaker adsorption. This can be rationalized in an orbital picture. If the metal d-orbitals lie low, it would produce a stable bonding orbital upon hybridization with the molecular orbitals of the adsorbate. However, in consequence, it would also produce relatively low-lying antibonding orbitals. When electrons fill up to the Fermi level, this would result in higher occupancy of these antibonding orbitals leading to a lower bond order.



(a) (b)

Figure 7: (a) A schematic of d-band model of adsorption and (b) calculated d-band center of Ru(0001) and Ru(1015) surfaces.

To study the adsorption phenomena according to this paradigm, the d-band centers of relaxed, isotropically compressed and expanded Ru(0001) and Ru(1015) surfaces were calculated and summarized as Figure 7(b). This shows that expansion pushes the d-band center to higher energy level while compression leads the d-band to lower energy level. The d-band centers of anisotropically stressed systems were also calculated and found to be intermediate to their isotropically stressed analogues and for simplicity was not reported.

CO adsorption energies at different sites of relaxed, and isotropically stressed systems

are reported in Figure 8. It can be said that compression leads to weaker binding and expansion leads to stronger binding. As discussed above, the compression and expansion leads to a lower and higher d-band center, respectively. This shows that the d-band model of adsorption can qualitatively predict the effect of strain to adsorption.

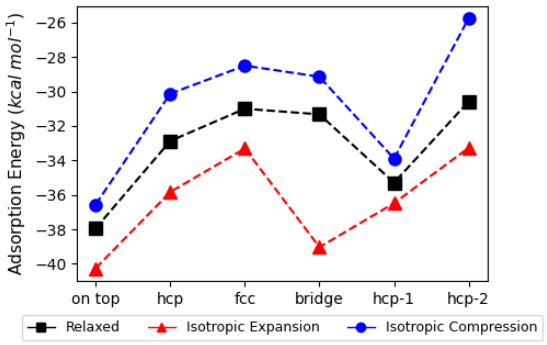


Figure 8: CO adsorption energies at different sites of Ru(0001) and Ru(1015) Surface. Dashed lines are added for visualization.

A recent paper demonstrated a new model called eigenstress model to (semi)quantitatively predict changes in binding energies.[27] According to this formalism, binding energy, E_{B}, changes due to strain, ϵ, can be summarized as

$$E_{\mathrm{B}}(\epsilon) = E_{\mathrm{B}}(0) + E_{\mathrm{int}}(\epsilon, \sigma) \tag{6}$$

where $E_{\mathrm{B}}(0)$ is the binding energy without strain, while $E_{\mathrm{int}}(\epsilon, \sigma)$ is the interaction energy between ϵ and σ and is defined as

$$E_{\mathrm{int}}(\epsilon, \sigma) = -\int_V \sum [\epsilon_{ij}(r)\sigma_{ij}(r)]dr \tag{7}$$

with ϵ and σ as the applied strain and adsorption eigenstress, respectively. The eigenstress is a tensor that accounts for the atomic level stress during adsorption, while the applied strain is the material level strain that can be introduced externally. The subscripts i, j accounts for the components of these tensor quantities.

As Eq. 7 is non-trivial to determine, a qualitative description can be generalized as

$$E_{\mathrm{B}}(\epsilon) \begin{cases} > E_{\mathrm{B}}(0) & \text{if } -\sum_{i,j} \epsilon_{ij}\sigma_{ij} > 0 \\ < E_{\mathrm{B}}(0) & \text{if } -\sum_{i,j} \epsilon_{ij}\sigma_{ij} < 0 \end{cases} \tag{8}$$

The above equation can be physically interpreted that if the applied strain to the system relieves the stress due to adsorption of the molecule, this would lead to stronger binding. Inversely, if the externally applied strain aggravates the adsorption-induced stress, this would lead to a weaker binding. To further simplify the discussion, take for example, Figure 9. In Figure 9(a), adatom pushes the surface atoms which induces a positive eigenstress at the surface. In order to relieve such stress, lattice expansion can be applied so that the system can relax. While in a system with a negative eigenstress such as the case in Figure 9(b), the adatom pulls the surface atoms. This type of stress can be relieved if a compressive strain is applied to the surface.

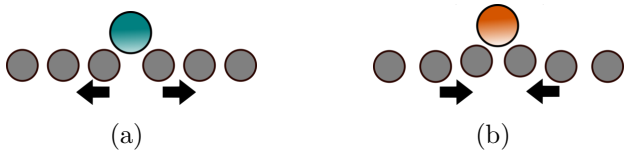
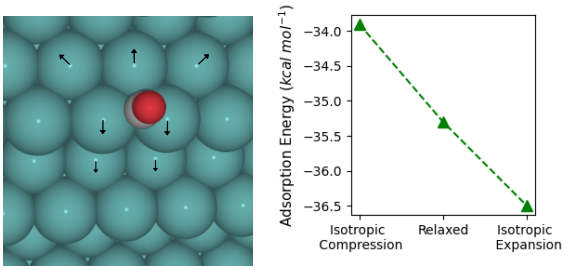


Figure 9: Schema of (a) positive eigenstress, and (b) negative eigenstress due to adsorbate. Adapted by permission from Springer Nature: Nature Catalysis (How strain can break the scaling relations of catalysis, A. Khorshidi et al), 2018.

To verify its effectiveness in predicting changes in adsorption energy, this model is applied in our system. In Figure 10(a), the CO induces a positive eigenstress to the Ru surface. According to the above discussion, lattice expansion would relieve the stress resulting in a more stable binding. This was observed in our calculations and is given as Figure 10(b).

In this case, both d-band model and eigenstress model were able to qualitatively predict the changes in the adsorption energies due to strain. Therefore, it can be said that eigenstress can be an alternative to d-band model. Furthermore, force calculation in eigenstress model is already part of the routine calculation while d-band center calculation requires a density of states calculation and a subsequent d-orbital projections. That is to say, eigenstress model is an inexpensive alternative to the d-band model. It should be noted, that



(a) (b)

Figure 10: Eigenstress Analysis. (a) Eigenstress, and (b) adsorption energy vs strain plot of CO adsorption in hcp-S1 site. CO adsorption produces positive eigenstress in (a) and positive lattice strain (expansion) is expected to augment adsorption which is observed in the calculated adsorption energy in (b). Red, gray, and green atoms are O, C, and Ru atoms, respectively.

in experiments, d-band center can be easily calculated. Hence, the use of eigenstress model would benefit computational chemistry guided catalyst design, rather than computational analysis of existing catalysts.

Reaction pathways in strained surface

To study CO decomposition in our models, we calculated six unique pathways given as Figure 11. These pathways are the most plausible subset from a previous study which focused on relaxed Ru surface.[36,51] Here, E_a and ΔE are calculated as

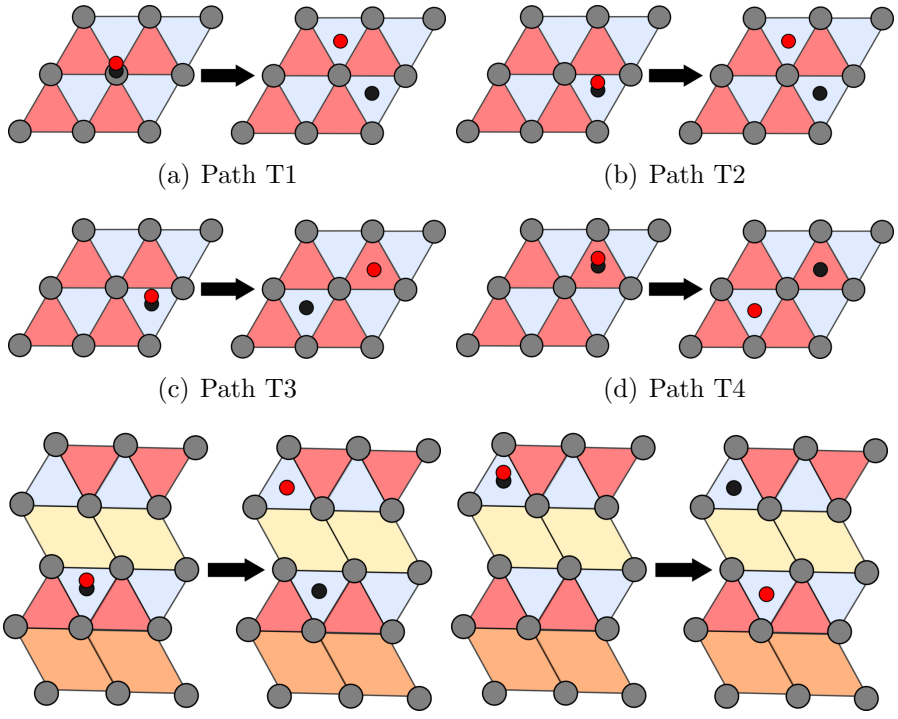
$$E_a = E_{TS} - E_R \tag{9}$$

$$\Delta E = E_P - E_R \tag{10}$$

where E_{TS}, E_R and E_P is the total electronic energy of the transition states, reactants and products described in Figure 11. In Path T1, CO initially sits on top of a Ru atom. At the converged minimum energy pathway, CO diffuses to the neighboring hcp site prior to dissociation. This observation was also found by Ciobica and van Santen.[36] To offer a discussion on this diffusion, we calculated the projected density of states (PDOS) of this

system. The PDOS and integrated PDOS of CO on on-top and hcp of Ru(0001) surface are given as Figures S36 and S37 of the SI, respectively. The DOS projected on CO molecular orbitals shows that the π^*-orbital which is the lowest unoccupied molecular orbital (LUMO) of the carbon monoxide increased in occupancy from 31.6% to 40.3% when moving from the on-top site to the hcp site. This prepares the CO molecule for the subsequent decomposition. Path T1 has a calculated activation energy of 56.94 kcal mol^{-1} while Path T2 has lower a calculated E_a of 51.85 kcal mol^{-1} where the CO is initially located at the hcp site. In the corresponding transition state, the O sits asymmetrically in a bridge and fcc site. Path T3 and T4 have activation energies of 59.94 kcal mol^{-1}, and 50.02 kcal mol^{-1}, respectively.

This is rationalized by the lesser stability of CO in the fcc site relative to hcp site.



(a) Path T1 (b) Path T2

(c) Path T3 (d) Path T4

(e) Path S1 (f) Path S2

Figure 11: CO dissociation pathways sampled in (a-d) terrace Ru(0001) and (e-f) stepped Ru(1015) surfaces. on-top (gray), hcp (blue), fcc (red). Red and black circles represent O and C atoms, respectively.

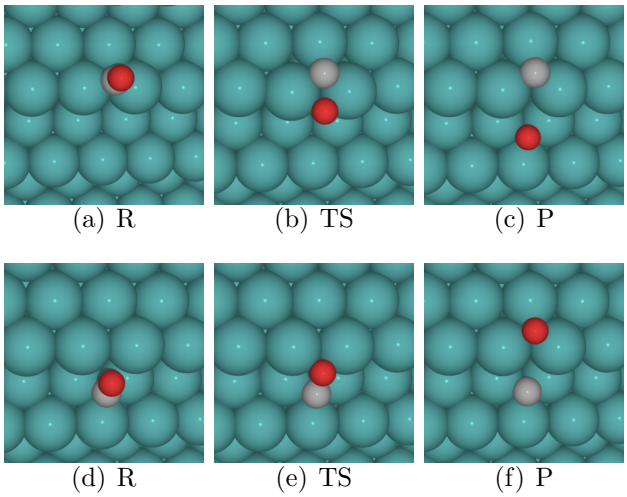
Activation energies from converged CI-NEB calculations are given as Table 3. This shows that the preferred pathway for CO dissociation in the Ru surface is Path S2 with calculated activation energy of 21.7 kcal mol^{-1}. This agrees with the known importance of the step

sites in FT reactions as well as the accepted CO dissociation pathway.[36]

The stability of this Path S2 over Path S1 can be associated with the transition state. The reactant, transition state, and product of Path S1 are illustrated as Figures 12(a), 12(b), and 12(c) and those of Path S2 as Figures 12(d), 12(e), and 12(f), respectively. As illustrated in Figure 12(e), the dissociating O is coordinated to two step-edge metal atoms. These atoms have a higher number of dangling bonds, and hence metal associated stabilization is expected. In contrast, such stabilization is not seen in Figure 12(b) since the C atom is located in the nearby *hcp* site and is also coordinated to the step-edge Ru atoms.

Table 3: Calculated activation and reaction energies from different reaction pathways in the relaxed Ru(0001) and Ru(1015) surfaces.

Surface	Path	E_a		ΔE	
		eV	kcal·mol $^{-1}$	eV	kcal· mol^{-1}
Ru(0001)	T1	2.47	56.9	0.64	14.8
	T2	2.25	51.9	0.42	9.7
	T3	2.60	59.9	0.42	9.7
	T4	2.17	50.0	0.62	14.3
Ru(1015)	S1	2.25	52.0	0.77	17.8
	S2	0.94	21.8	0.29	6.7



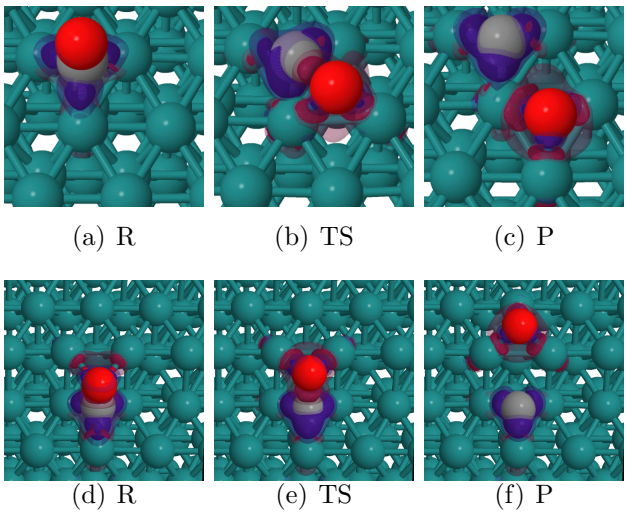
(a) R (b) TS (c) P

(d) R (e) TS (f) P

Figure 12: Optimized structures of reactants (R), transition states (TS), and products (P) in (a-c) Path S1 and (d-f) Path S2 in a relaxed Ru(1015) cell. Red, gray, and green atoms are O, C, and Ru atoms, respectively.

After determining dissociation reaction pathways in the relaxed Ru(0001) and Ru(1015)

surface, corresponding reaction pathways in isotropically and anisotropically strained surfaces were calculated. To characterize the binding, charge density difference (CDD) maps were calculated for adsorption complexes. The electron flow is qualitatively maintained in all cases as depicted in the CDD maps given as Figures S38-71 attached in the SI. As representative, CDD maps for systems without strain are given in Figure 13. This is expected as external force induced geometry changes do not change the electronic characteristic of an atom.



(a) R (b) TS (c) P

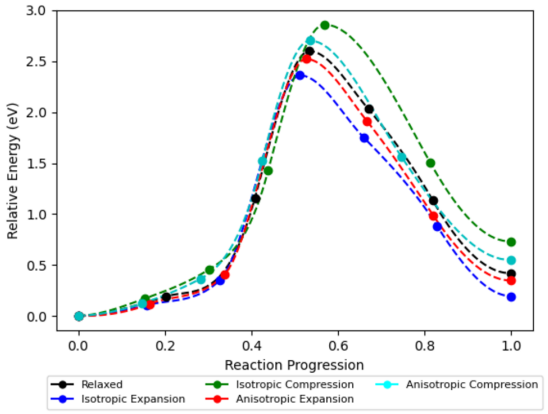
(d) R (e) TS (f) P

Figure 13: Charge Density Difference plots of reactants (R), transition states (TS), and products (P) of (a-c) Path T2 in terrace Ru(0001), and (d-f) Path S2 in stepped Ru(1015). Red, gray, and green atoms are O, C, and Ru atoms, respectively. Red and blue isosurfaces show increase and decrease of negative charge, respectively. Isosurfaces with isovalues of 0.01 and 0.005 are shown simultaneously with decreasing opacity.

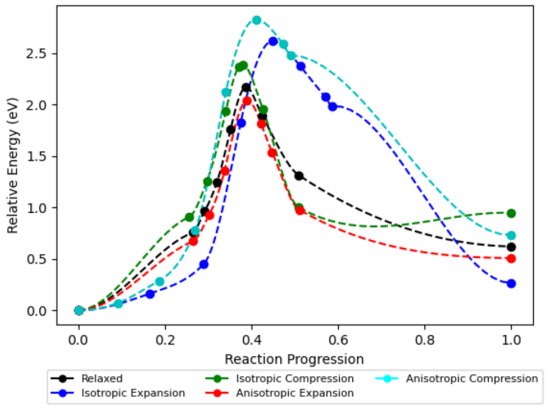
Bader charges also show a similar trend for other cases as seen in Figures S72-77 in the SI. However, as electron distribution changes due to conformation, the magnitude of Bader charge differs with each case showing dependence on dissociation path and slab.

The effect of strain in Path T3 is given as Figure 14(a) where it can be easily seen that it follows scaling relation —that is the reaction energies and activation energies scale with each other.[52] Interestingly, expansion shows higher stabilization leading to a lower activation energy and reaction energy while compression shows the opposite trend. Similar observations are seen in other paths and corresponding CI-NEB profiles are appended as Figures S78-83 in

the SI. This was expected from the seminal paper of Nørskov and colleagues which discusses the effect of strain, which lead to the current paradigm in strain effects in heterogeneous catalysis.[53]



(a)



(b)

Figure 14: CI-NEB pathways for (a) Path T3 and (b) Path T4 in terrace Ru(0001) surfaces.

However, this is not the case in Path T4. A notable change in the minimum energy pathway is shown in Figure 14(b). At a relaxed state, the dissociation path starts with the diffusion of CO to a neighboring hcp site. Then, CO tilts until the CO bond is broken. In comparison, at an isotropically expanded Ru(0001) surface, the reaction proceeds directly from the fcc site through an over the hill transition state structure. The optimized structure of chemical reaction relevant extrema is shown in Figure 15. This shows that the strain—as a mechanochemical concept—changes the minimum energy pathway. Naturally, a change

in the minimum path is an exemption to BEP and TSS scaling relations. Hence, reaction energy and activation energy of this pathway do not show a linear relation.

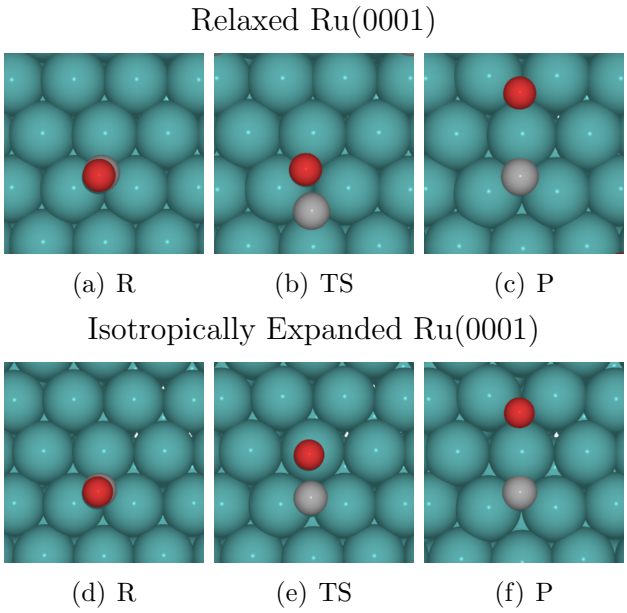
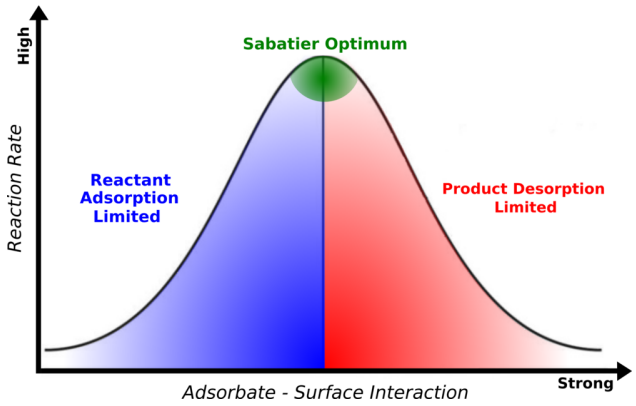


Figure 15: Optimized structures of reactants (R), transition states (TS), and products (P) in path T4 in (a-c) relaxed and (d-f) isotropically expanded Ru(0001) cell. Red, gray, and green atoms are O, C, and Ru atoms, respectively.

Another important concept in heterogeneous catalysis and a consequence of scaling relation is the Sabatier principle which is illustrated as Scheme 1. This principle asserts that there is an optimum amount of slab interaction to attain optimum turn-over frequency. The kinetics of the reaction would be hindered by strong binding via a lowered product desorption. On the other hand, weak interaction to the surface would lead to inefficient activation of reaction.

The premise of the Sabatier principle is that the adsorption energy of the reactant to the surface is directly proportional to the activation energy of the reaction. In Path S2, 3% compression leads to a lower activation energy with a weaker adsorption as seen in Figure 16(a).

This curious result can be rationalized by the interaction energy with respect to the slab. Interaction energy is calculated as



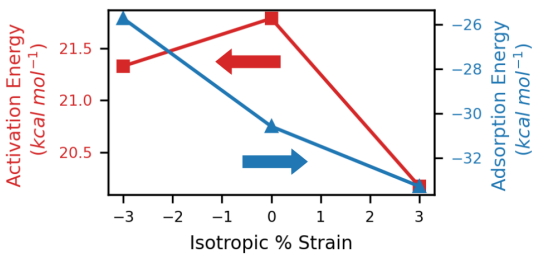
Scheme 1: Schematic of Sabatier principle.

$$E_{\text{int}} = E_{\text{complex}} - E_{\text{CO}}^{\text{complex}} - E_{\text{slab}}^{\text{complex}} \tag{11}$$

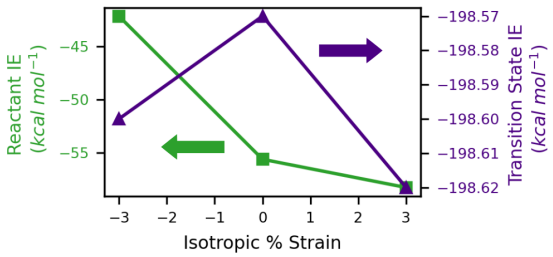
where E_{complex} is the total energy of the system, $E_{\text{CO}}^{\text{complex}}$ and $E_{\text{slab}}^{\text{complex}}$ is the total energy of CO and slab at the complex geometry, respectively.

Figure 16(b) shows that the trend in activation energy follows the trend in transition state interaction energy. It should also be noted that the reactant interaction energy follows that of adsorption. This shows that the slab contribution in stabilizing the transition state is different to that of the reactant which is seen as the different trend in adsorption and activation energies. In such cases, the Sabatier principle is not followed. This exemption to the rule is not unique to our chemical model and results. In a comprehensive paper of Foppa, Copéret, and Comas-Vives which highlighted the nanoparticle (NP) size effect to the CO decomposition activity of ruthenium, they found out that NP size induces a break in the scaling relations which they attributed to the surface curvature of the NP.[54] In a microscopic view, the curvature of the nanoparticle affects the interatomic spacing in the surface which can be attributed to a mechanical strain brought by the NP size.

To discuss the physical relevance of Figure 16(b), we will take the isotropically expanded case as reference where we define the ratio of adsorbed CO and dissociating CO to be equal. In comparison to the reference, the relaxed slab which has higher activation energy as shown



(a)



(b)

Figure 16: (a) Adsorption energy (Red) in hcp-2 site and activation energy of Path S2 (Blue) of Ru(1015) surface as function of strain and (b) interaction energy of reactant (green) and transition state (magenta) in hcp-2 site of Ru(1015) surface as function of strain.

in Figure 16(a) would have more molecular CO adsorbed to the surface than those proceeding to the dissociation reaction. The compressed Ru(1015) would correspond to a system with a higher ratio of dissociated CO than the currently adsorbed CO. This break in relation may potentially lead to a more efficient catalyst for CO decomposition using Ru and other Fischer-Tropsch related metal systems such as copper, iron, and corresponding alloys.

Conclusions

In this work, the potential of isotropic and anisotropic strain in heterogeneous catalysis was explored. Specifically, the strain effects on the activity of terrace Ru(0001), and stepped Ru(1015) surfaces towards CO dissociation reaction was put in focus. Initially, the CO adsorption energies were calculated and found that on-top site was preferred. Using the stepped surface, the step-edge site was preferred which follows classical understanding of

unsaturated dangling bonds.

The effect of the applied strain on the adsorption energy is well predicted by the d-band center model. The lowering of the d-band center during compression resulted in a lower adsorption energy. Tensile strain has the exact opposite effect following the d-band model. In addition to this, the novel eigenstress model also provided the same prediction on the effect of external strain to CO adsorption.

In general, the electron flow remains qualitatively the same during adsorption and dissociation. This was supported by the similar Charge Density Difference plots in each slab. Trends in Bader charges are also the same. Compression afforded higher Bader charges which signifies higher electron donation due to compressive strain.

There are several notable effects of surface strain to the calculated minimum energy pathway. Some pathways remained the same and their corresponding energies scales according to BEP and TSS relationships. On the other hand, the Path T4 in the Ru(0001) surface proceeded through a different transition state. This effectively changes the CI-NEB path and its energetics.

Furthermore, the adsorption scaling relation was also broken in the case of an isotropically compressed Ru(1015) model. Activation energy was found to decrease rather than increase as expected by the BEP relation. This decrease is associated with the change in the interaction energy in the reactant and transition state complexes. This is another instance that the scaling relation in heterogeneous catalysis can be broken due to applied strain.

The findings of this research exemplified the utility of mechanical stress to create new reaction pathways. This also opens an escape from the adsorption scaling relation in heterogeneous catalysis. Though compression allows lower CO dissociation activation energy with respect to adsorption energy, the expected speed up for the Fischer-Tropsch reaction needs to be validated by kinetic simulations or by experiments.

Supporting Information Available

Poisson Ratio Calculation. Murnaghan Equation of State. Optimized structures of reactant, transition state, and products for CO dissociation in Relaxed and strained terrace Ru(0001) surface. Optimized structures of reactant, transition state, and products for CO dissociation in Relaxed and strained stepped Ru(1015) surface. Results of Bader Charge analysis for CO dissociation pathways. Charge density difference maps of optimized structures. Projected Density of States (PDOS and Integrated PDOS for the selected reactants states. Converged Minimum Energy Pathways for CO dissociation in Ru(0001) and Ru(1015) surfaces.

Acknowledgement

This work was financially supported by Japan Society for the Promotion of Science (JSPS) KAKENHI Grant-in-Aid for Scientific Research (B) (No.JP20H02685), and Ministry of Education, Culture, Sports, Science and Technology (MEXT) Project (Integrated Research Consortium on Chemical Sciences). This research was also partly supported by the Photo-excitonix Project from Hokkaido University. Part of the computations were carried out at RCCS (Okazaki, Japan).

References

(1) Coulson, E. A. The Fischer–Tropsch Process. *Nature* **1950**, *166*, 533.

(2) Dry, M. E. The Fischer–Tropsch process: 1950–2000. *Catal. Today* **2002**, *71*, 227–241, Fischer-Tropsch synthesis on the eve of the XXI Century.

(3) Shetty, S.; Jansen, A. P. J.; van Santen, R. A. Direct versus Hydrogen-Assisted CO Dissociation. *J. Am. Chem. Soc.* **2009**, *131*, 12874–12875.

(4) van Helden, P.; van den Berg, J.-A.; Ciobîcă, I. M. Hydrogen-assisted CO dissociation on the Co(211) stepped surface. *Catal. Sci. Technol.* **2012**, *2*, 491–494.

(5) Loveless, B. T.; Buda, C.; Neurock, M.; Iglesia, E. CO Chemisorption and Dissociation at High Coverages during CO Hydrogenation on Ru Catalysts. *J. Am. Chem. Soc.* **2013**, *135*, 6107–6121.

(6) Hibbitts, D. D.; Loveless, B. T.; Neurock, M.; Iglesia, E. Mechanistic Role of Water on the Rate and Selectivity of Fischer–Tropsch Synthesis on Ruthenium Catalysts. *Angew. Chem., Int. Ed. Engl.* **2013**, *52*, 12273–12278.

(7) Hibbitts, D.; Dybeck, E.; Lawlor, T.; Neurock, M.; Iglesia, E. Preferential activation of CO near hydrocarbon chains during Fischer–Tropsch synthesis on Ru. *J. Catal.* **2016**, *337*, 91–101.

(8) Vendelbo, S. B.; Johansson, M.; Mowbray, D. J.; Andersson, M. P.; Abild-Pedersen, F.; Nielsen, J. H.; Nørskov, J. K.; Chorkendorff, I. Self Blocking of CO Dissociation on a Stepped Ruthenium Surface. *Top. Catal.* **2010**, *53*, 6107–6121.

(9) Ge, Q.; Neurock, M.; Wright, H. A.; Srinivasan, N. A First Principles Study of Carbon—Carbon Coupling over the {0001} Surfaces of Co and Ru. *J. Phys. Chem. B* **2002**, *106*, 2826–2829.

(10) Shetty, S.; van Santen, R. A. Hydrogen induced CO activation on open Ru and Co surfaces. *Phys. Chem. Chem. Phys.* **2010**, *12*, 6330–6332.

(11) Liu, J.-X.; Wang, P.; Xu, W.; Hensen, E. J. Particle Size and Crystal Phase Effects in Fischer-Tropsch Catalysts. *Engineering* **2017**, *3*, 467–476.

(12) Lyu, S.; Wang, L.; Li, Z.; Yin, S.; Chen, J.; Zhang, Y.; Li, J.; Wang, Y. Stabilization of ϵ-iron carbide as high-temperature catalyst under realistic Fischer–Tropsch synthesis conditions. *Nat. Commun.* **2020**, *11*, 2041–1723.

(13) Xu, K.; Sun, B.; Lin, J.; Wen, W.; Pei, Y.; Yan, S.; Qiao, M.; Zhang, X.; Zong, B. ϵ-Iron carbide as a low-temperature Fischer–Tropsch synthesis catalyst. *Nat. Commun.* **2014**, *5*, 2041–1723.

(14) Li, Y.; Li, Z.; Ahsen, A.; Lammich, L.; Mannie, G. J. A.; Niemantsverdriet, J. W. H.; Lauritsen, J. V. Atomically Defined Iron Carbide Surface for Fischer–Tropsch Synthesis Catalysis. *ACS Catal.* **2019**, *9*, 1264–1273.

(15) Andersson, M.; Abild-Pedersen, F.; Remediakis, I.; Bligaard, T.; Jones, G.; Engbæk, J.; Lytken, O.; Horch, S.; Nielsen, J.; Sehested, J. et al. Structure sensitivity of the methanation reaction: H2-induced CO dissociation on nickel surfaces. *J. Catal.* **2008**, *255*, 6–19.

(16) Engbæk, J.; Lytken, O.; Nielsen, J. H.; Chorkendorff, I. CO dissociation on Ni: The effect of steps and of nickel carbonyl. *Surf. Sci.* **2008**, *602*, 733–743.

(17) Chen, W.; Filot, I. A. W.; Pestman, R.; Hensen, E. J. M. Mechanism of Cobalt-Catalyzed CO Hydrogenation: 2. Fischer–Tropsch Synthesis. *ACS Catal.* **2017**, *7*, 8061–8071.

(18) Pestman, R.; Chen, W.; Hensen, E. Insight into the Rate-Determining Step and Active Sites in the Fischer–Tropsch Reaction over Cobalt Catalysts. *ACS Catal.* **2019**, *9*, 4189–4195.

(19) Zijlstra, B.; Broos, R. J. P.; Chen, W.; Oosterbeek, H.; Filot, I. A. W.; Hensen, E. J. M. Coverage Effects in CO Dissociation on Metallic Cobalt Nanoparticles. *ACS Catal.* **2019**, *9*, 7365–7372.

(20) Yang, J.; Tveten, E. Z.; Chen, D.; Holmen, A. Understanding the Effect of Cobalt Particle Size on Fischer—Tropsch Synthesis: Surface Species and Mechanistic Studies by SSITKA and Kinetic Isotope Effect. *Langmuir* **2010**, *26*, 16558–16567.

(21) Shi, J.; Chen, L.-Q. Strain Engineering in Functional Materials. *J. Appl. Phys.* **2019**, *125*, 082201.

(22) Greeley, J. Theoretical Heterogeneous Catalysis: Scaling Relationships and Computational Catalyst Design. *Annu. Rev. Chem. Biomol. Eng.* **2016**, *7*, 605–635.

(23) Wang, S.; Vorotnikov, V.; Sutton, J. E.; Vlachos, D. G. Brønsted–Evans–Polanyi and Transition State Scaling Relations of Furan Derivatives on Pd(111) and Their Relation to Those of Small Molecules. *ACS Catalysis* **2014**, *4*, 604–612.

(24) Liu, F.; Wu, C.; Yang, G.; Yang, S. CO Oxidation over Strained Pt(100) Surface: A DFT Study. *J. Phys. Chem. C* **2015**, *119*, 15500–15505.

(25) Asano, M.; Kawamura, R.; Sasakawa, R.; Todoroki, N.; Wadayama, T. Oxygen Reduction Reaction Activity for Strain-Controlled Pt-Based Model Alloy Catalysts: Surface Strains and Direct Electronic Effects Induced by Alloying Elements. *ACS Catal.* **2016**, *6*, 5285–5289.

(26) Temmel, S. E.; Fabbri, E.; Pergolesi, D.; Lippert, T.; Schmidt, T. J. Investigating the Role of Strain toward the Oxygen Reduction Activity on Model Thin Film Pt Catalysts. *ACS Catal.* **2016**, *6*, 7566–7576.

(27) Khorshidi, A.; Violet, J.; Hashemi, J.; Peterson, A. A. How strain can break the scaling relations of catalysis. *Nat. Cal.* **2018**, *263*, 2520–1158.

(28) Weissmüller, J. Mechanochemistry breaks with expectations. *Nat. Cal.* **2018**, *1*, 238–239.

(29) Norskov, J.; Studt, F.; Abild-Pedersen, F.; Bligaard, T. *Fundamental Concepts in Heterogeneous Catalysis*; John Wiley & Sons, Inc, Hoboken, New Jersey, 2014; Chapter 8, pp 114–137.

(30) Enkovaara, J.; Rostgaard, C.; Mortensen, J. J.; Chen, J.; Dułak, M.; Ferrighi, L.; Gavnholt, J.; Glinsvad, C.; Haikola, V.; Hansen, H. A. et al. Electronic structure calculations with GPAW: a real-space implementation of the projector augmented-wave method. *J. Phys.: Condens. Matter* **2010**, *22*, 253202.

(31) Mortensen, J. J.; Hansen, L. B.; Jacobsen, K. W. Real-space grid implementation of the projector augmented wave method. *Phys. Rev. B* **2005**, *71*, 035109.

(32) Enkovaara, J.; Romero, N. A.; Shende, S.; Mortensen, J. J. GPAW - massively parallel electronic structure calculations with Python-based software. *Procedia Computer Science* **2011**, *4*, 17–25, Proceedings of the International Conference on Computational Science, ICCS 2011.

(33) Larsen, A. H.; Mortensen, J. J.; Blomqvist, J.; Castelli, I. E.; Christensen, R.; Dułak, M.; Friis, J.; Groves, M. N.; Hammer, B.; Hargus, C. et al. The atomic simulation environment—a Python library for working with atoms. *J. Phys.: Condens. Matter* **2017**, *29*, 273002.

(34) Hammer, B.; Hansen, L. B.; Nørskov, J. K. Improved adsorption energetics within density-functional theory using revised Perdew-Burke-Ernzerhof functionals. *Phys. Rev. B* **1999**, *59*, 7413–7421.

(35) Lehtola, S.; Steigemann, C.; Oliveira, M. J. T.; Marques, M. A. L. Recent developments in libxc – A comprehensive library of functionals for density functional theory. *SoftwareX* **2018**, *7*, 1–5.

(36) Ciobica, I. M.; van Santen, R. A. Carbon Monoxide Dissociation on Planar and Stepped Ru(0001) Surfaces. *J. Phys. Chem. B* **2003**, *107*, 3808–3812.

(37) Ciobica, I. M.; Kleyn, A. W.; Van Santen, R. A. Adsorption and Coadsorption of CO and H on Ruthenium Surfaces. *J. Phys. Chem. B* **2003**, *107*, 164–172.

(38) Pulay, P. Convergence acceleration of iterative sequences. the case of scf iteration. *Chemical Physics Letters* **1980**, *73*, 393–398.

(39) Kresse, G.; Furthmüller, J. Efficient iterative schemes for ab initio total-energy calculations using a plane-wave basis set. *Phys. Rev. B* **1996**, *54*, 11169–11186.

(40) Monkhorst, H. J.; Pack, J. D. Special points for Brillouin-zone integrations. *Phys. Rev. B* **1976**, *13*, 5188–5192.

(41) Groß, A. *Theoretical Surface Science: A Microscopic Perspective 2nd Edition*; Advanced Texts in Physics; Springer-Verlag Berlin Heidelberg, 2009; pp 68–69.

(42) Filot, I. A. W.; van Santen, R. A.; Hensen, E. J. M. Quantum chemistry of the Fischer–Tropsch reaction catalysed by a stepped ruthenium surface. *Catal. Sci. Technol.* **2014**, *4*, 3129–3140.

(43) Zijlstra, B.; Broos, R. J. P.; Chen, W.; Bezemer, G. L.; Filot, I. A. W.; Hensen, E. J. M. The Vital Role of Step-Edge Sites for Both CO Activation and Chain Growth on Cobalt Fischer–Tropsch Catalysts Revealed through First-Principles-Based Microkinetic Modeling Including Lateral Interactions. *ACS Catal.* **2020**, *10*, 9376–9400.

(44) Samsonov, G. *Handbook of the Physicochemical Properties of the Elements*; IFI/Plenum, Washington, New York, 1968; p 396.

(45) Murnaghan, F. D. Finite Deformations of an Elastic Solid. *Am. J. Math* **1937**, *59*, 235–260.

(46) Murnaghan, F. D. The Compressibility of Media under Extreme Pressures. *Proc. Natl. Acad. Sci. U. S. A.* **1944**, *30*, 244–247.

(47) Jain, A.; Ong, S. P.; Hautier, G.; Chen, W.; Richards, W. D.; Dacek, S.; Cholia, S.; Gunter, D.; Skinner, D.; Ceder, G. et al. The Materials Project: A materials genome approach to accelerating materials innovation. *APL Mater.* **2013**, *1*, 011002.

(48) Berne, B. J.; Ciccotti, G.; Coker, D. F. *Classical and Quantum Dynamics in Condensed Phase Simulations*; World Scientific, 1998.

(49) Henkelman, G.; Uberuaga, B. P.; Jónsson, H. A climbing image nudged elastic band method for finding saddle points and minimum energy paths. *J. Chem. Phys.* **2000**, *113*, 9901–9904.

(50) Smidstrup, S.; Pedersen, A.; Stokbro, K.; Jónsson, H. Improved initial guess for minimum energy path calculations. *J. Chem. Phys.* **2014**, *140*, 214106.

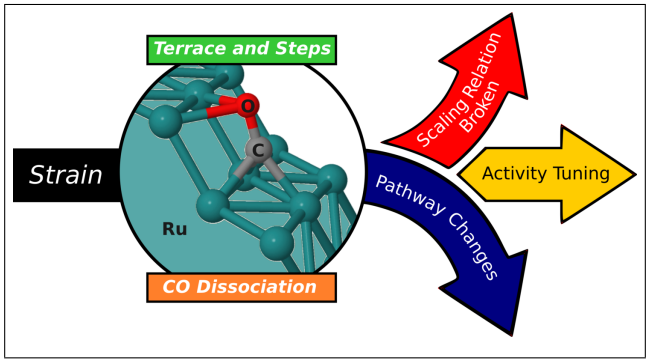
(51) Shetty, S.; van Santen, R. A. CO dissociation on Ru and Co surfaces: The initial step in the Fischer–Tropsch synthesis. *Catal. Today* **2011**, *171*, 168–173.

(52) Norskov, J.; Studt, F.; Abild-Pedersen, F.; Bligaard, T. *Fundamental Concepts in Heterogeneous Catalysis*; John Wiley & Sons, Inc, Hoboken, New Jersey, 2014; Chapter 6, pp 85–96.

(53) Mavrikakis, M.; Hammer, B.; Nørskov, J. K. Effect of Strain on the Reactivity of Metal Surfaces. *Phys. Rev. Lett.* **1998**, *81*, 2819–2822.

(54) Foppa, L.; Copéret, C.; Comas-Vives, A. Increased Back-Bonding Explains Step-Edge Reactivity and Particle Size Effect for CO Activation on Ru Nanoparticles. *J. Am. Chem. Soc.* **2016**, *138*, 16655–16668.

TOC Graphic


Terrace and Steps
Strain
O
C
Ru
CO Dissociation
Scaling Relation Broken
Activity Tuning
Pathway Changes